J. Jpn. Soc. Powder Powder Metallurgy, **72** (2025) S1241-S1248
https://doi.org/10.2497/jjspm.16C-T11-10

Novel Lightweight Design of Additively Manufactured Structural Components through Biomimetics

Tim RÖVER[1*], Tjark SIEVERS[1], Karim ASAMI[1], Claus EMMELMANN[1]

[1]Hamburg University of Technology, Institute of Laser and Systems Technology, Harburger Schloßstraße 28, 21079 Hamburg, Germany

Abstract

PBF-LB/M offers efficient production of complex and functional metal components. Research shows that the mechanical performance of components can be enhanced by incorporating biomimetic shapes, such as banana pseudo stem-inspired biomimetic beams. This work addresses three mechanical topology optimization problems, using AlSi10Mg. Leveraging these models, novel component designs featuring biomimetic beams and novel node designs were developed based on the input topology optimization. The new biomimetic component designs were compared to their topology optimization counterparts that were used as references. Numerical analyses of mass and structural integrity were performed to evaluate improvements. Lightweight biomimetic component designs for additively manufactured components were developed using the developed methods. Weight savings of 12.5-30.3 % were achieved compared to the input topology optimization results. However, further research on the design methodologies is needed to ensure that the mechanical stress criterion is also met within the nodes of the generated biomimetic designs.

Keywords: Design for additive manufacturing (DfAM), powder bed fusion of metal with laser beam (PBF-LB/M), aluminum alloy AlSi10Mg, biomimetics, lightweight design

1. Introduction

The combination of laser additive manufacturing and biomimetics resulted in numerous efficient component designs [1–3]. However, the use of biomimetics in Additive Manufacturing (AM) is still limited. One of the limiting factors are missing design tools [1]. This study presents a detailed methodology for biomimetic design of mechanical components from topology optimization (TO) results to partly close this gap in research. A study compared the conventional design of an aircraft bracket with a newly developed design of the bracket that combined additive manufacturing and biomimetics [4]. An initial design of the bracket was generated by TO. In the next step, a bamboo-inspired structure was introduced to improve the parts lightweight character. The authors state, that a change of the material, manufacturing technique and design resulted in a weight reduction of 50 % when comparing the newly developed part with the original part [4]. Based on this approach a methodology for integration of biomimetic beams in TO results was developed [5]. The methodology focuses on mechanical TO results that are truss-like and consist of members and nodes. The authors suggest five conceptual design steps on how to advance such a TO result to a biomimetic component design [5]. Building on this approach a detailed abstraction methodology [6] and a design tool for biomimetic beams under bending were presented in other studies. A research gap is given by a missing detailed solution for node design that is in line with the method from Röver et al. [5] and application of the resulting full design process to exemplary TO results. Therefore, the goal of this paper is to close this research gap.

2. Materials and Methods

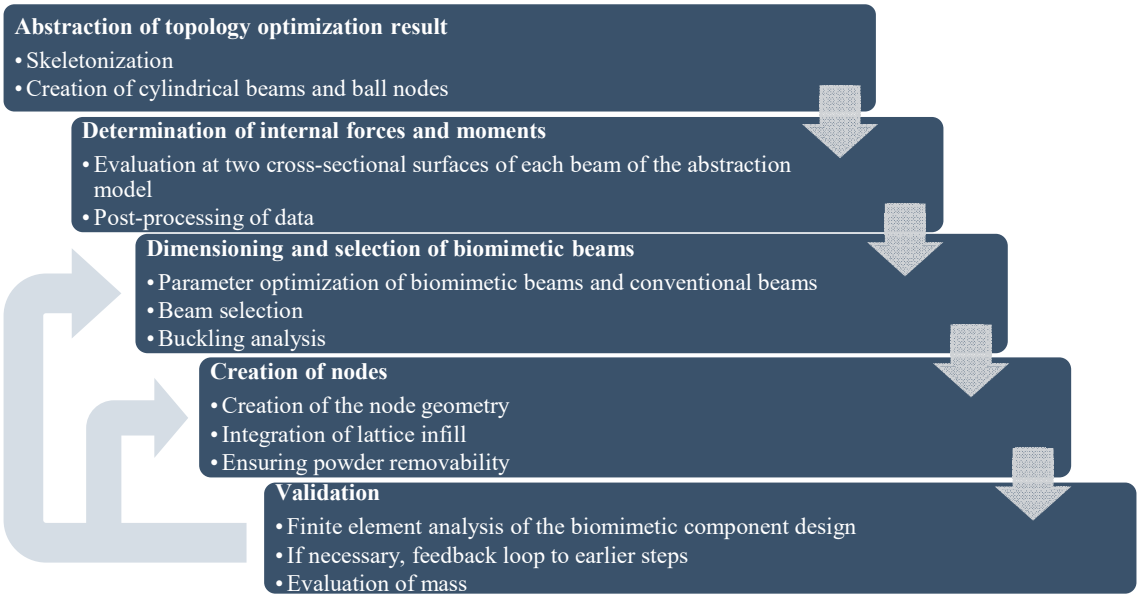

Fig. 1. Flowchart of methodology for development of additively manufactured structural components through biomimetics based on topology optimization results.

*corresponding author, E-mail: tim.roever@tuhh.de

Fig. 1 shows the flowchart of the design methodology that was developed and applied within this work. It is based on the previous study [5] and focuses on the powder bed fusion of metal with laser beam (PBF-LB/M) process as the AM process of choice due to its great relevance in industry. The proposed methodology involves a comprehensive five-step approach to optimize and validate biomimetic structures that are developed from TO results. The first step, abstraction of TO results, employs skeletonization to derive a simplified model consisting of cylindrical beams and ball nodes. This abstraction facilitates the determination of internal forces and moments in the second step, where evaluations are conducted at two cross-sectional surfaces of each beam, followed by data post-processing. The third step focuses on dimensioning and selecting biomimetic beams. This includes parameter optimization for both biomimetic and conventional beams, beam selection, and conducting a buckling analysis. The creation of nodes in the fourth step involves developing node geometries, integrating lattice infills, and ensuring good powder removability, which is crucial for the PBF-LB/M process. Finally, the validation step encompasses Finite Element Analysis (FEA) of the biomimetic component design to verify structural integrity. If the stress criterion (acceptance criterion) is not satisfied, a feedback loop allows for iterative refinement of earlier steps. Additionally, the evaluation of mass allows comparison of the biomimetic design with the original TO design. Heat-treated AlSi10Mg was considered as a material in this study. Material properties can be found in Table 1 and are based on literature [7–9]. Comsol Mutliphysics 6.0 [10], Autodesk Inventor 2024 [11] and nTop 4.22.2 [12] are the software that were used in this work.

Table 1 Material properties of heat-treated AlSi10Mg manufactured by PBF-LB/M. Adapted from literature [7] (licensed under CC BY 4.0).

Material Property	Value
Yield strength	141 MPa [8]
Young's modulus	57 GPa [8]
Poisson's ratio	0.34 [9]
Density	2.67 g/cm^3 [8]

3. Results

In this section the results of the study are presented.

A. Reference Topology Optimization Results and Abstractions

The TO results and abstractions used in this work were taken from a previous study [6] and its corresponding data set [13]. The study [6] considered structural steel as material for all components. In contrast, aluminum alloy AlSi10Mg (see Table 1) was considered for all components in this study. Due to the manufacturing restrictions of the PBF-LB/M process such as minimum wall thicknesses and minimum distances between opposing walls, it was assumed that larger components would have a greater potential for improvement in terms of lightweighting. Therefore, the TO results and abstractions were scaled up. The size of the respective TO results and abstractions was increased by factors of 4, 4, and 1.5 for the Michell cantilever, the Messerschmitt-Bölkow-Blohm (MBB) beam and the L-shape, respectively (see Fig. 7 (a)-(c)). Certain PBF-LB/M systems have relatively large build envelopes with dimensions of e.g. 500 mm × 280 mm × 850 mm [14]. Therefore, all upscaled designs fit into the build envelope of such PBF-LB/M systems. Furthermore, the abstraction of the Mitchell cantilever was complemented by adding two beams (see #15 and #16 in Fig. 7 (f)) that connect the abstraction with the mechanical support.

Based on the changes, the mechanical loads of the upscaled TO designs had to be increased to allow for a meaningful comparison to the biomimetic designs later on in the study (see Table 3). For identification of suitable forces, the TO results (see Fig. 7 (a)-(c)) were considered. For each result, the force that would lead to a maximum von Mises stress of 80 % inside the component, was identified by a numerical parameter optimization study in COMSOL Multiphysics 6.0. It is noted that stresses were not evaluated close to the perfectly stiff supports as well as close to the surfaces to which the forces were applied. This approach prevents evaluating physically meaningless stress peaks that are caused by discretization of the mechanical problem. The identified loads can be found in Table 2.

Table 2 Geometric scaling factors and identified loads for design study

Model	Geometric scaling factor	Load [N]
Michell cantilever	4	8237.5
MBB beam	4	16044
L-shape	1.5	2981

B. Evaluation of Internal Forces and Moments

For evaluation of internal forces and moments of the abstractions (see Fig. 7 (d)-(f)), FEAs were performed in COMSOL Multiphysics 6.0. The upscaled mechanical boundary conditions were considered. Furthermore, for each beam, work planes were added if possible at 20 % of the beam length and at 80 % of the beam length according to the study by Röver et al. [5]. If two beams intersected at an acute angle, a work plane might intersect with a neighboring beam. In such cases the work plane was moved towards the center of the beams away from the intersection of beams (see Fig. 2) to prevent that evaluation planes would intersect with neighboring beams. According to literature [6], the section forces function as implemented in COMSOL Multiphysics 6.0 was used for all evaluation planes. Doing so for each evaluation plane the axial force N, the shear force along the first local axis T_1, the shear force along the second local axis T_2, the twisting moment M_t, the bending moment around the first local axis M_1, and the bending moment around the second local axis M_2 could be identified.

According to literature it can be assumed that N, T_1, T_2, and M_t are constant along the length of the beams [5]. Due to numerical discretization of the mechanical problem usually small deviations are present when comparing the numerical values that were evaluated at the planes at 20 % of the length and at 80 % of the length of the beams. In these cases, the average of the two values was used as an approximation for the next steps of the methodology.

M_1 and M_2 cannot be assumed to be constant along the length of the beams. The bending moments within each beam occur from the shear forces and the bending moments applied to the ends of the beams. It can be assumed that the bending moments that occur at the cross-sections of the beams change linearly with respect to the beam length [5]. Using the bending moments values evaluated at each of

the two planes of a beam, the bending moment values are extrapolated to 0 % and 100 % of the length of the respective beam using a spreadsheet. This approach is in line with one of the previous studies on this method [5].

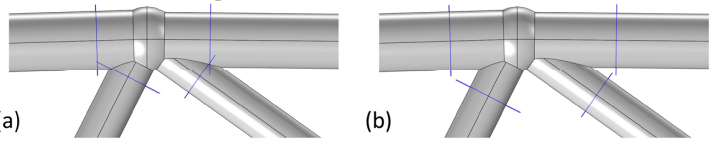

Fig. 2. Exemplary critical node with planes for evaluation of internal forces and moments in abstractions. (a) planes for evaluation at 20 % and 80 % of lengths of beams that intersect with planes of neighboring beams; (b) alternative and preferred locations of planes for evaluation.

C. Dimensioning and Selection of Biomimetic Beams

Dimensioning and selection of beams in this work was based on the study by Röver et al. [7] and the respective dataset [15]. The work provides parametric designs of beams and parameter optimization models for dimensioning of the beams under bending loads. Fig. 3 (a), (c) and (d) show the parametric cross-section designs of solid cylindrical beam (SC), revolver drum beam 1 (RD1) and revolver drum beam 2 (RD2) according to the study, respectively. It is noted, that the design parameter intervals as provided by the authors of the study, consider manufacturing restrictions of the PFB-LB/M process. The three previously existing designs were augmented in this study by a parametric design of a hollow cylindrical beam (HC) that is shown in Fig. 3 (b). Based on the parametric HC design a corresponding parameter optimization model of the HC was developed that is analogous to the existing models with respect to the finite element mesh, the optimization settings and the mechanical constraints.

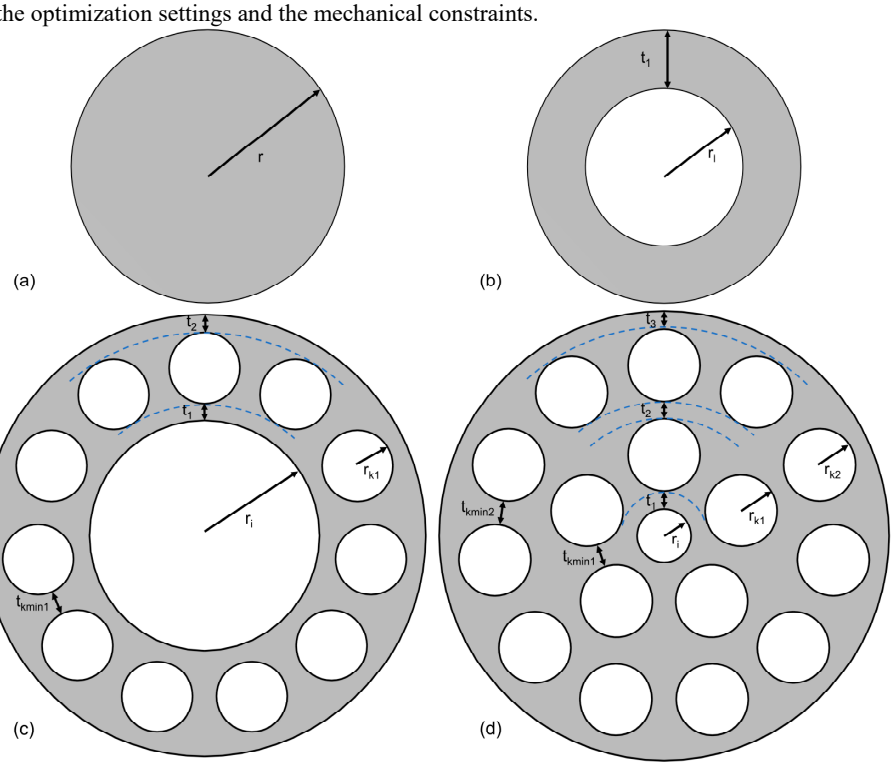

Fig. 3. Parametric beam designs. (a) solid cylindrical beam (SC); (b) hollow cylindrical beam (HC); (c) revolver drum beam 1 (RD1); (d) revolver drum beam 2 (RD2). Adapted and partly reprinted from literature [7] (licensed under CC BY 4.0).

The models from the work by Röver et. al. [7] are fixed to a length of 100 mm and considered a shear force resulting in a bending moment only. They are mechanically fixed at one end and have a boundary force acting at their free end. The optimization models minimize the cross-sectional area of the beams while considering certain constraints.

The parametric models of SC, HC, RD1 and RD2 were improved in this paper. The meshing sequence was improved such that the number of elements increases with respect to the length of the beam. Based on the work by Röver et. al. [7] the element length in direction of the main axis of the beam was set to approximately one millimeter. Furthermore, to achieve more accurate numerical results, the element length in direction of the main axis of the beam was halved for the elements close to the mechanical support as well as the elements close to the boundary where the forces and moments are applied. Additionally, the models were augmented by using the rigid connector function in COMSOL Multiphysics 6.0, to efficiently apply forces and moments to the free ends of the beams. The parameter optimization models in this work allow for application of an axial force, a shear force along the first local axis, a shear force along the second local axis, a twisting moment, a bending moment around the first local axis, and a bending moment around the second local axis.

The upper limits for occurring von Mises stresses in the domains of interest of all parameter optimization models were modified to 80 % of the yield strength of AlSi10Mg, which is 112.8 MPa (see also Table 1). The RD2 design has a minimum outer diameter of 21 mm considering the defined parameter intervals. Therefore, to reduce computational efforts within the study, RD2 optimizations were only run for a beam, if the result of the RD1 optimization gave a beam with an outer diameter larger than 21 mm.

Fig. 4 shows optimization results of all four types of beams based on the evaluated forces and moments and the length of one exemplary cylindrical beam of the abstraction of a TO result. Therefore, all four beams are subject to the same mechanical boundary conditions and have the same length. It can be seen that regions of high stress in all results are close to the maximum allowable stress of 112.8 MPa. In the next step, the beam that has the lowest cross-sectional area is chosen. This value can be evaluated in the optimization models with low effort and compared in a spreadsheet.

To ensure structural integrity of the selected beams, beams that are under compression have to be analyzed with regard to buckling. For this step, buckling analysis is done in COMSOL Multiphysics 6.0 using the same material parameters, the same mechanical boundary conditions and the same meshing sequence as was used for the final result of the corresponding parameter optimization. By evaluation of the critical load factors, it can be estimated whether or not the beams might be unstable with regard to buckling. If the lightest of the four beams is uncritical with regard to buckling, it is chosen. If a beam is found to be critical with regard to buckling, the following iterations are performed: Increase of the wall thickness of the outermost ring (parameter r of SC design, parameter t_1 for HC design, parameter t_2 for RD1 design and parameter t_3 for RD2 design) by small increments. Identification of a small value of the respective parameter for that the beam design is not critical with regard to buckling according to buckling analysis. Doing so, one valid solution for the respective beam can be found. The same may be done for the other three beams. Then again, the beam with the lowest cross-sectional area is chosen for the next steps of the methodology. It is noted that not all four beams have to be investigated that way, if one initial solution of a beam is uncritical to buckling. In this case, beams with higher cross-sectional areas do not need to be investigated in this way. Alternatively, if a SC beam is found to be critical with regard to buckling, dimensioning may be done using the Euler buckling criterion considering a fixed-free condition according to literature [16,17].

After all final beam designs were selected, the beams are introduced into a new component in COMSOL Multiphysics 6.0. The beams are oriented based on the orientation of beams in the abstraction of the TO. Furthermore, it has to be ensured that their orientation (rotation about main axis of beam) is in line with the optimization simulations, as RD1 and RD2 designs are not fully rotationally symmetric. Additionally, sheet-like elements are added in regions where supports are located and in regions were loads are applied in the original TOs. In preparation of the step of node generation, all beams are shortened such that the beams do not intersect and additionally have a certain distance between them that allows for a smooth node. The outcome of this step for the three components investigated in this work can be seen in Fig. 7 (g)-(i). These preliminary component designs are exported in Standard for the Exchange of Product model data (STEP)-file format.

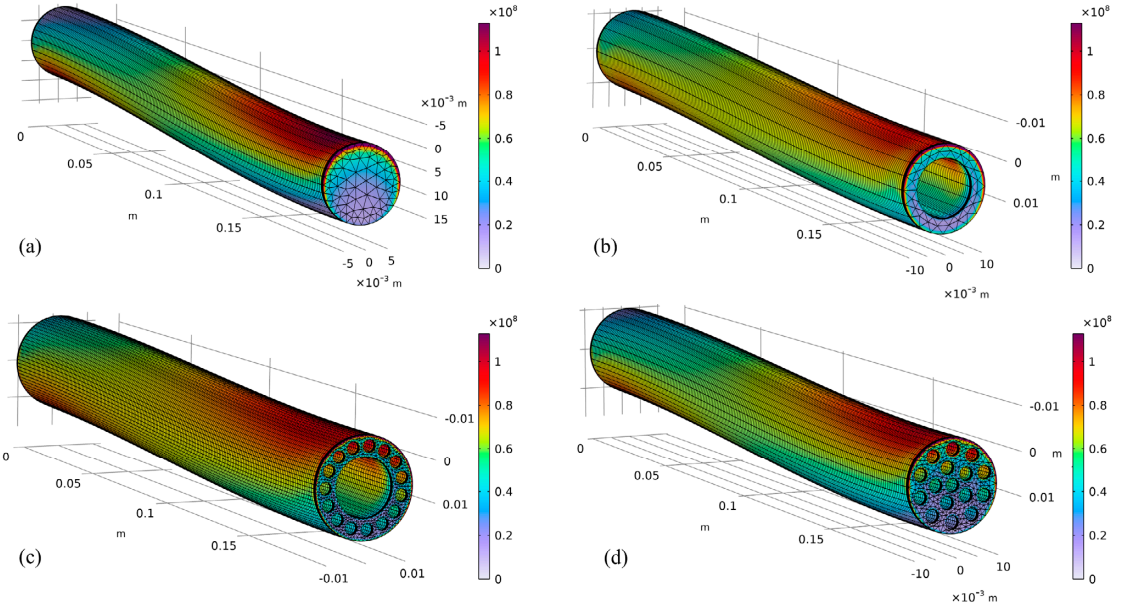

Fig. 4. Exemplary finite element method-based parameter optimization results of beams subject to the same mechanical boundary conditions. Deformation of the beams are exaggerated for improved visibility. (a) solid cylindrical beam (SC); (b) hollow cylindrical beam (HC); (c) revolver drum beam 1 (RD1); (d) revolver drum beam 2 (RD2).

D. Generation of Nodes

Röver et al. suggest TO for generation of lightweight node designs [5]. As generation of high-quality TO results often requires a lot of time, effort, and, experienced engineers are needed, a different approach was followed in this study. For this study, the following goals were defined for development of a methodology for node design between the optimized beams: 1. Transmission of forces and moments between beams, 2. Ensure structural integrity, 3. Ensure powder removability from node as well as cavities of beams connected to node, 4. Ensure that node design and resulting final component design consider manufacturing restrictions of PBF-LB/M, 5. Small mass of node, and 6. Ensure that design sequence of nodes is robust and time-efficient. One promising approach for node design was found to be the use of lattice structures. Certain lattice structures were found to be well suited with regards to powder removability and were found to show high potential for lightweight design [18]. Furthermore, many lattice structures are self-supporting in PBF-LB/M. Node generation was performed in two steps: the generation of solid volume nodes and the integration of lattice infill structure into the nodes.

For generation of the solid volume nodes Autodesk Inventor 2024 was used. The corresponding design steps based on an exemplary node are depicted in Fig. 5. First the STEP-file containing the optimized beams and sheet-like elements is imported into the software.

Then, the following steps are carried out for all nodes: First, a 2 mm offset is added to the outer diameter of the end of the beam that is facing towards the node. This is done for all beams of the node (see Fig. 5 (a)). In the next step, the loft function is used to connect the offset circles of all beams of a node with each other (see Fig. 5 (b), (c)&(d)). After using the loft function, a node may have one or more holes near its center. If so, the sketch function and extrusion function are used to generate a solid volume at the center of the nodes, closing any holes. The extrusion thickness is based on the outer radii of the beams connected to the node. Next, the fillet function is used for smoothing of the node (see Fig. 5 (e)&(f)). Smoothing is also done in direction of the center parts of the beams such that additional material is added to the beams. Then the node geometry is separated from the beams by cuts using work planes (see Fig. 5 (g)&(h)). To achieve the final solid volume node, extruded cuts of the cavities of the beams into the node are done (see Fig. 5 (i)). The length of the extruded cuts is suggested to be equal or greater than the later used unit cell size of the lattice structure. Then a single STEP-file is exported, that contains the whole component geometry including beams and nodes. The beams and nodes are defined as solid volumes within the STEP-file.

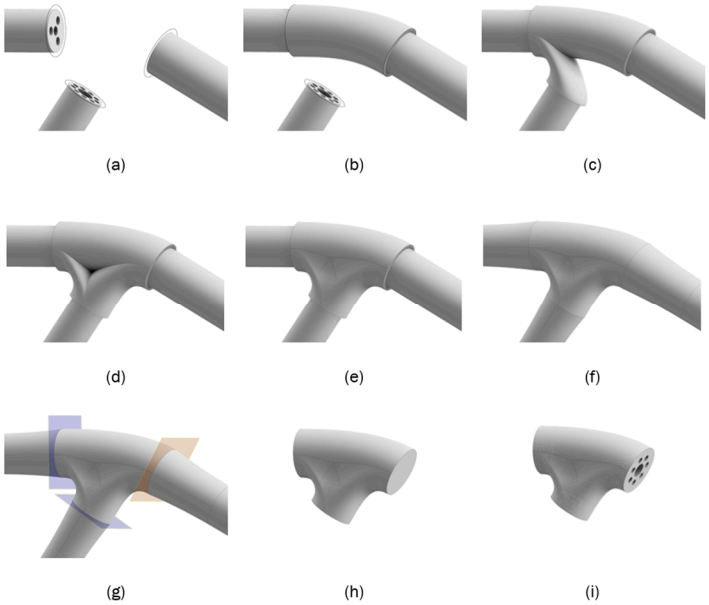

Fig. 5. Generation of an exemplary solid volume node in five steps. (a) added offsets; (b), (c)&(d) connection of all beams; (e)&(f) smoothing; (g)&(h) separation of node; (i) extrusion of cavities into nodes.

For integration of the lattice infill structures into the nodes and finalization of the node design, nTop 4.22.2 is used. First, the STEP-file is imported to nTop. Next, the nodes and beams of the design are converted to implicit bodies. Then the following steps are carried-out for all nodes (see Fig. 6): First a shell is generated from the solid volume (see Fig. 6 (a)) and perforations are added to further modify the shell (see Fig. 6 (b)). Shell wall thicknesses of 3 mm provided good results for many nodes generated in this study. Next, circular cut-outs are added for powder removal to achieve the final shell of the node (see Fig. 6 (c)). Next, the solid volume of the initial node is filled with a Kelvin cell to generate a lattice structure (see Fig. 6 (d)&(e)). The design parameters of the Kelvin cell should be chosen in such a way that powder can be removed through the structure and manufacturing constraints of PBF-LB/M are considered. In this work Kelvin cells with unit cell size of 5 mm × 5 mm × 5 mm and a thickness value between 2 mm and 2.5 mm were used. In the final step, the shell of the node and its lattice infill are combined to obtain the final node design (see Fig. 6 (f)&(g)). By application of this method lattice-filled nodes can be generated.

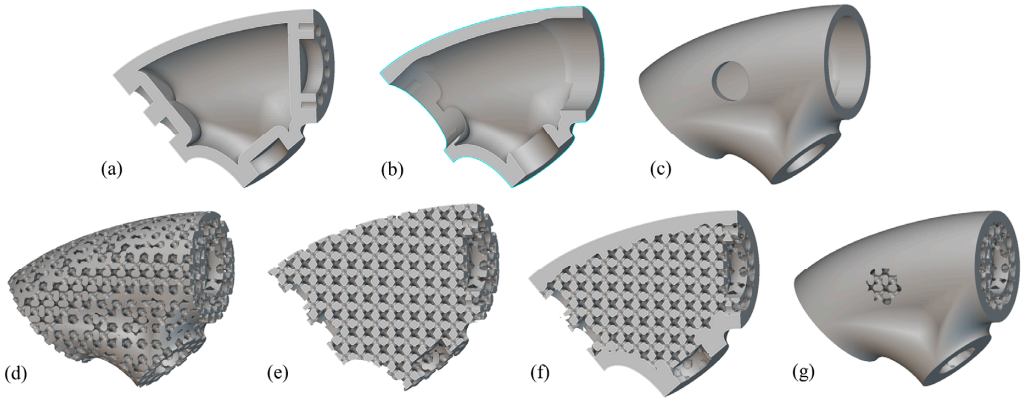

Fig. 6. Generation of an exemplary lattice-filled node in five steps. (a) section view of first generation of shell; (b) section view of second generation of shell; (c) shell with circular cut-outs for powder removal; (d) Kelvin lattice structure in bounds of original node; (e) section view of Kelvin lattice structure in bounds of original node; (f) section view of final lattice-filled node; (g) final lattice-filled node.

E. Complete Biomimetic Designs

The modification of nodes and introduction of infill structures according to the previous section can be accomplished in nTop, thereby enabling the generation of a complete component design that incorporates biomimetic beams and lattice-filled nodes. It is noted that the generation of the complete biomimetic designs of the three components exhibits certain unique aspects, which are outlined in the following paragraphs.

In the beam optimizations of all three component designs, selected parameters were restricted using additional upper bounds to reduce the computational effort. For SC parameter r was additionally restricted, for HC parameter t_1 was additionally restricted, for RD1 t_1 and t_2 were additionally restricted and for RD2 t_1, t_2 and t_3 were additionally restricted. This was necessary to achieve optimization results within an acceptable time frame. The final optimization results show that the values of the respective design parameters are considerably lower than the chosen upper bounds for all cases. Therefore, it can be expected that the additional restriction of the solution space had no negative impact on the optimization results.

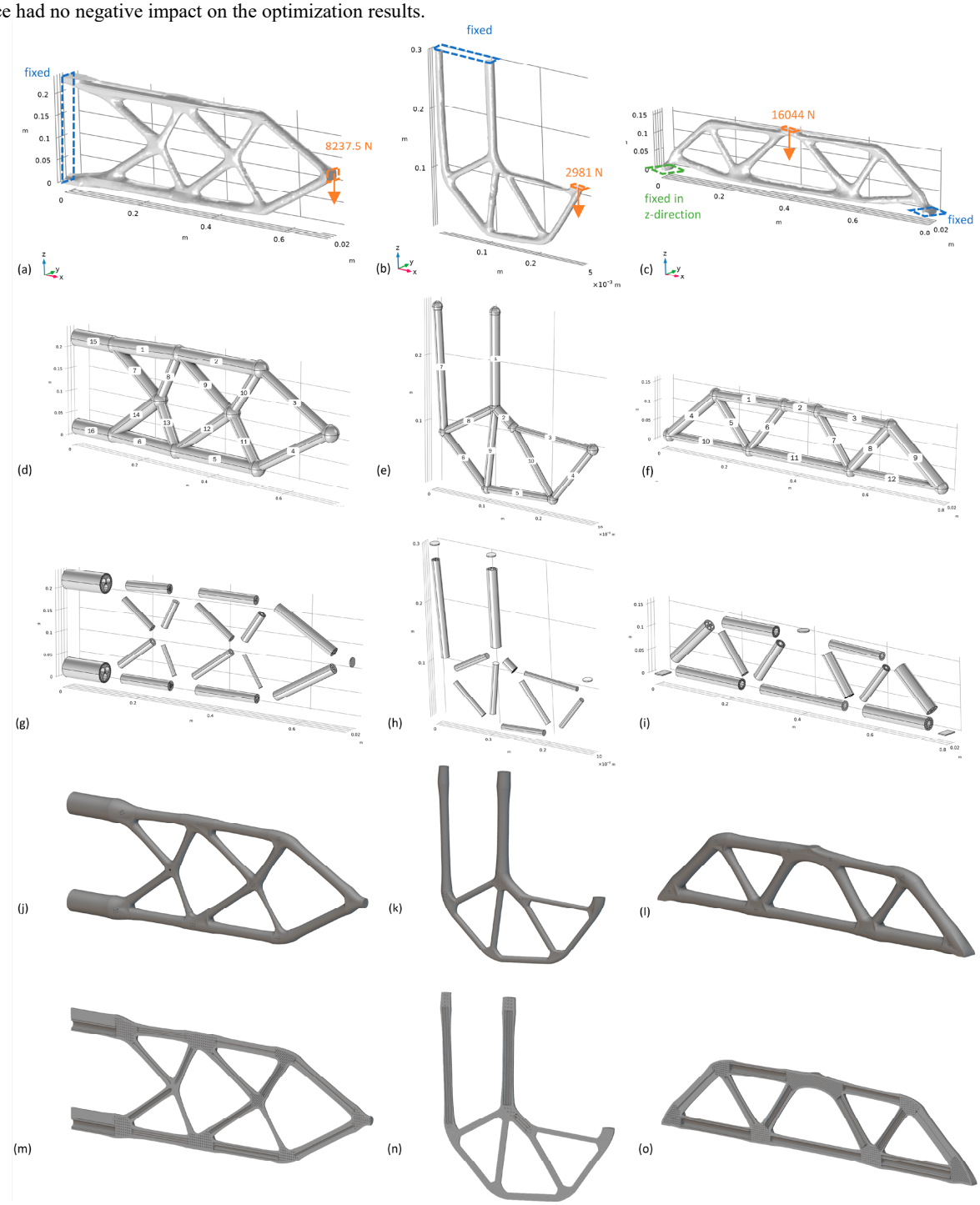

Fig. 7. Views of reference topology optimization results, interim results and final component designs of Michell cantilever, L-shape and MBB beam. (a)-(c): topology optimization results with boundary conditions. (d)-(f): abstractions of topology optimization results. (g)-(i): arrangements of biomimetic beams. (j)-(l): final biomimetic component designs. (m)-(o): section views of final biomimetic component designs.

The L-shape contains seven SC beams. As SC beams do not have cavities, removal of internal powder is not necessary. The nodes linking SC beams were generated using a modified design approach. During generation of the solid volume nodes, no 2 mm offsets were added to the outer diameter of the end of SC beams. Furthermore, if a node connected only SC beams no lattice infill was used,

but solid volume nodes were generated. For nodes that connect SC beams with other kinds of beams, a lattice structure was used in those areas of the node that connect beams with cavities. Regions of the nodes close to SC beams were designed as solid volumes if lattice structure was not necessary for powder removal. This modified design approach was used to ensure better powder removability and provide more material in the nodes close to the SC beams that are solid themselves for an increased structural integrity. Furthermore, the L-shape was the only component of the three components in which beams under compressive loads were found to be critical with regard to buckling. All three critical beams were SC beams. According to the presented methodologies the Euler buckling criterion was used for dimensioning of SC beams. Subsequent buckling analysis of the newly dimensioned SC beams yielded no risk for buckling. Additionally, when comparing the updated beams with the other beams of the same load case, they were still the lightest and, therefore, used for the final component design.

During application of the design methodology, beam #2 of the MBB beam (see Fig. 7 (f)) was omitted as it was relatively short. Also, the sheet element where the force is applied, was integrated into the node.

In the implementation of the design methodology for the Michell cantilever, one node was designed on an individual basis, diverging from the presented design methods. For this node that connects one SC beam and three HC beams, an alternative node design without a lattice structure was employed. A solid volume node was generated and openings from the HC cavities to the exterior were added with the loft function in Autodesk Inventor 2024. Moreover, in the case of the Michell cantilever, the SC, the HC and the RD2 beam optimizations were conducted for selected beam load cases, only, thus reducing the computational effort in this part of the study. Furthermore, RD2 was preselected and optimized for beams #15 and #16 to reduce the computational effort.

The complete biomimetic component designs can be found in Fig. 7 (j)-(o). The biomimetic Michell cantilever features all four types of beams, whereas the biomimetic MBB beam only features HC and RD1 beams. The biomimetic L-shape mostly utilizes SC beams and three RD1 beams.

F. Finite Element Analysis of the Biomimetic Component Designs

FEAs of the three biomimetic component designs were conducted. A component design would be considered mechanically acceptable (acceptance criterion), if the von Mises stresses did not exceed the yield strength of the material (141 MPa). At the same time good comparability to the TO designs would be given if the von Mises stress did not exceed 80 % of the yield strength of the material (112.8 MPa) as this threshold was used for scaling of the force values with the scaled TO results.

Fig. 8 shows a section view of the biomimetic MBB beam. It can be seen that in multiple nodes in the finite element mesh 80 % of the yield strength of the material is exceeded (these nodes are highlighted in blue). It can be seen that the critical areas are rather small and are located at the unions of the nodes and the beams. Additionally, a small number of critical nodes were located in the central parts of certain nodes. Variation of the node design parameters including the choice of the type of lattice structure was done. However, no design could be generated which satisfied the acceptance criterion. Also, the biomimetic Michell cantilever showed areas in which the yield strength of the material was exceeded. Critical regions were located at the unions of the nodes and the beams, regions inside the nodes including the lattice structures of the nodes, regions close to supports and regions close to where forces were applied. In the case of the L-shape, the yield strength of the material was exceeded at unions of the nodes and the beams as well as certain regions inside the nodes.

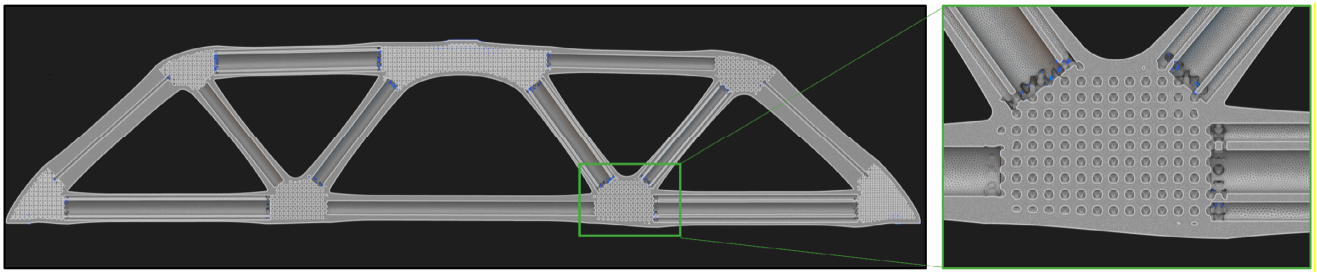

Fig. 8. Section view and detail view of final MBB beam biomimetic component designs. Nodes in which the von Mises stress exceeds 80 % of the yield strength of the material (112.8 MPa) are highlighted in blue.

Furthermore, the yield strength of the material was exceeded in regions close to supports and regions close to where forces are applied. Also, for the Michell cantilever and the L-shape variation of the node design parameters was done. However, also for these components no designs could be generated which satisfied the acceptance criterion. Thus, all three biomimetic designs could not satisfy the acceptance criterion based on the yield strength of the material. At the same time, it could be shown that the biomimetic beams in all design were well dimensioned based on the utilized methodology.

Table 3 Comparison of mass of topology optimization designs and biomimetic component designs

Component design	Mass [g]	Weight reduction compared to topology optimization result
Michell cantilever – topology optimization	3069.3	-
Michell cantilever - Biomimetic	2139.7	30.3 %
MBB beam - topology optimization	2220.4	-
MBB beam - Biomimetic	1889	14.9 %
L-shape - topology optimization	384.6	-
L-shape - Biomimetic	336.5	12.5 %

G. Assessment of the Lightweight Performance

For assessment of the lightweight performance of the biomimetic component designs, their masses were evaluated. Furthermore, the mass of each of the TO results was evaluated. Comparison of biomimetic designs with original TO results yielded a weight reduction of 30.3 %, 14.9 % and 12.5 % for Michell cantilever, MBB-beam and L-shape, respectively. Results of evaluation are summarized in Table 3.

4. Discussion

The research gap addressed by this study could be partly closed as a detailed solution for node design was developed that is in line with the method from [5]. Furthermore, an application of the full design process to three exemplary TO results was done such that three biomimetic component designs were generated. Improvement of a design that was generated by well-performed TO is a challenging task, as such a result is a mathematical optimum. Therefore, the weight reductions of 12.5-30.3 % compared to the original TO results that were achieved in this study show the great potential of the utilized approach and the developed methods. The design methods show high potential for a fast and cost-efficient design of lightweight components that are produced by PBF-LB/M and may contribute to a more sustainable mobility in sectors such as automotive and aerospace. FEA of the biomimetic designs yielded that von Mises stresses exceeded the yield strength of the material in certain nodes in all of the three components. Efforts to find alternative design solutions for the nodes have so far been unsuccessful. Therefore, the proposed design methodology could not be validated successfully. Even though the acceptance criterion could not be satisfied, the developed designs show a high potential as only the nodes in the biomimetic component designs were critical in terms of the occurring von Mises stresses. The authors assume that the design methodology could be improved to achieve better node designs. A focus should be put on an improved transition between node designs and beam designs as well as achieve a lattice structure that prevents peak stresses more efficiently. This may achieve overall component designs that satisfy the stress criterion. At the same time, the authors of this study believe that it is possible to achieve mechanically improved nodes that have approximately the same weight as the current designs but satisfy the stress criterion. Therefore, this study contributes to closing the addressed research gap and presents interim results on node design for biomimetic components as well as identifies node design as one aspect that should be addressed in future works.

5. Conclusions and Future Prospects

This study focused on the advancement, application and assessment of design methodologies for additively manufactured biomimetic structural components. A design methodology for node design of biomimetic structural components was developed. The methodology builds on previous works in this field. Furthermore, the previously existing design methodologies and the newly developed methodology were combined and applied to three TO results to achieve novel biomimetic structural components. FEA showed that in all biomimetic component designs, stresses above the yield strength of the material occurred. Therefore, the design criterion could not be satisfied. At the same time comparison of biomimetic designs with the original TO results yielded a weight reduction of between 12.5 and 30.3 %. Therefore, valuable design solutions and the great potential of the design approach could be demonstrated in this study. Future research should aim to enhance the node design methodology in order to develop an overarching design methodology that can satisfy the stress criterion during the application of the aforementioned methodologies while achieving low component masses.

References

1. Gralow, M., Weigand, F., Herzog, D., Wischeropp, T. & Emmelmann, C. Biomimetic design and laser additive manufacturing—A perfect symbiosis? *Journal of Laser Applications* **32**, 021201 (2020).
2. Du Plessis, A. *et al.* Beautiful and Functional: A Review of Biomimetic Design in Additive Manufacturing. *Additive Manufacturing* **27**, 408–427 (2019).
3. Yang, Y. *et al.* Recent Progress in Biomimetic Additive Manufacturing Technology: From Materials to Functional Structures. *Advanced Materials* **30**, 1706539 (2018).
4. Emmelmann, C., Petersen, M., Kranz, J. & Wycisk, E. Bionic lightweight design by laser additive manufacturing (LAM) for aircraft industry. in *SPIE Eco-Photonics 2011: Sustainable Design, Manufacturing, and Engineering Workforce Education for a Green Future* (eds. Ambs, P. et al.) 80650 (SPIE, 2011). doi:10.1117/12.898525.
5. Röver, T. *et al.* Methodology for Integrating Biomimetic Beams in Abstracted Topology Optimization Results. in *Proceedings of the ASME 2022 International Mechanical Engineering Congress and Exposition. Volume 4: Biomedical and Biotechnology; Design, Systems, and Complexity* (Columbus, Ohio, USA, 2022). doi:10.1115/IMECE2022-94299.
6. Röver, T., Bader, M., Asami, K., Emmelmann, C. & Kelbassa, I. Development and assessment of a methodology for abstraction of topology optimization results to enable the substitution of optimized beams. *Journal of Laser Applications* **35**, (2023).
7. Röver, T., Fuchs, C., Asami, K. & Emmelmann, C. Dimensioning of Biomimetic Beams under Bending for Additively Manufactured Structural Components. *Biomimetics* **9**, 214 (2024).
8. SLM Solutions Group AG. Material Data Sheet Al-Alloy AlSi10Mg.
9. Sert, E. *et al.* Tensile strength performance with determination of the Poisson‘s ratio of additively manufactured AlSi10Mg samples. *Materialwiss. Werkstofftech.* **50**, 539–545 (2019).
10. COMSOL. COMSOL Multiphysics - Reference Manual - Version: 6.0. (2021).
11. Autodesk Inc. Inventor 2024 Help | Inventor API User’s Manual | Autodesk. https://help.autodesk.com/view/INVNTOR/2024/ENU/?guid=UserManualIndex.
12. nTopology Inc. Next-Gen Engineering Design Software: nTop (formerly nTopology). *nTop* https://www.ntop.com/.
13. Röver, T., Bader, M., Asami, M. K., Emmelmann, C. & Kelbassa, I. Supplementary material to article with title: Development and Assessment of a Methodology for Abstraction of Topology Optimization Results to Enable the Substitution of Optimized Beams. https://doi.org/10.15480/882.8168 (2023).
14. SLM Solutions Group AG. SLM®800 Brochure - Selective Laser Melting Machine - Large Format Selective Laser Melting.
15. Röver, T., Fuchs, C., Asami, M. K. & Emmelmann, C. Parameter Optimization Files (COMSOL Multiphysics 6.0) for Dimensioning of Biomimetic Beams under Bending. https://doi.org/10.15480/882.9113 (2024).
16. *Technische Mechanik. 2: Elastostatik / Dietmar Gross, Werner Hauger, Jörg Schröder, Wolfgang A. Wall*. (Springer Vieweg, Berlin; [Heidelberg], 2017). doi:10.1007/978-3-662-53679-7.
17. Euler, L. *Methodus Inveniendi Lineas Curvas Maximi Minimive Proprietate Gaudentes, Sive Solutio Problematis Isoperimetrici Lattissimo Sensu Accepti*. (Lausannæ & Genevæ, 1744).
18. Tao, W. & Leu, M. C. Design of lattice structure for additive manufacturing. in *2016 International Symposium on Flexible Automation (ISFA)* 325–332 (IEEE, Cleveland, OH, USA, 2016). doi:10.1109/ISFA.2016.7790182.

Received July 2, 2024; Revised October 17, 2024; Accepted October 21, 2024